Nonlinear Dynamics (2026) 114:557
https://doi.org/10.1007/s11071-026-12429-4

RESEARCH

Localized structures close to translational symmetry-breaking point: noise-induced transitions to run-and-tumble motion

Fernando R. Humire[1] · Karin Alfaro-Bittner[2,3] · Marcel G. Clerc[4] · René G. Rojas[5]

Received: 21 August 2025 / Revised: 5 February 2026 / Accepted: 27 February 2026

Abstract

Macroscopic systems can exhibit particle-type solutions such as solitary waves, pulses, vegetation patches, and front solutions, among others. These localized structures may show active-like behavior when reflection symmetry is broken and fluctuations are present. Here, we investigate a one-dimensional non-variational system with multiplicative noise in which initially motionless structures drift and stochastically reverse their direction, resembling the run-and-tumble motion of bacteria. For low noise level intensities, the mean square displacement of the localized structure position displays a predominantly ballistic regimen with bimodal position distributions, while at high noise levels induce more frequent switching and complex transport dynamics, including initial diffusion, intermediate ballistic, and long-term diffusion regimes. A minimal model for the position and velocity captures run-and-tumble dynamics with rates governed by a Kramers law. The associated Fokker–Planck equation reproduces the full dynamics across all time scales, confirming the noise-induced transition in velocity and the diffusive behavior in position for long times. These findings show that active-like behavior can arise in nonlinear systems through both parity-breaking symmetry and noise.

Keywords Localized structures · Run-and-tumble motion · Spontaneous symmetry-breaking · Noise

1 Introduction

Localized structures are robust confined spatial solutions that emerge in a wide variety of extended nonlinear systems, such as reaction-diffusion models, fluid dynamics, and optical media [1–7]. In this context, one of the most striking phenomena is the emergence of particle-like behaviors, in which the localized structure (LS) not only maintains its spatial confinement but also acquires dynamic properties such as mobility, propagation direction, or polarity [1–8]. These solutions can be described by continuous parameters, such as position, and discrete parameters that encode characteristics such as charge, symmetry, or width. An equally paradigmatic and historical case is that of solitons, first observed in water channels [9–11], whose dynamics and understanding were key to the understanding of particle-type solutions and field theory [12], as well as the development of optical telecommunications [13]. In recent decades, this concept has been extended beyond conservative systems to dissipative media, where such solutions are usually called dissipative solitons or localized structures [3–7, 14]. These have been observed in a wide variety of physical contexts, including magnetic domains, chiral bubbles in liquid crystals, current

✉ Fernando R. Humire
f.humire@academicos.uta.cl

Karin Alfaro-Bittner
karin.alfaro@urjc.es

Marcel G. Clerc
marcel@dfi.uchile.cl

René G. Rojas
rene.rojas@pucv.cl

1 Departamento de Física, Facultad de Ciencias, Universidad de Tarapacá, Casilla 7-D, Arica, Chile

2 Universidad Rey Juan Carlos, Calle Tulipán s/n, 28933 Móstoles, Madrid, Spain

3 Data, Complex Networks and Cybersecurity Sciences Technological Institute, Universidad Rey Juan Carlos, Plaza ManuelBecerra 14, 28028 Madrid, Spain

4 Departamento de Física and Millennium Institute for Research in Optics, FCFM, Universidad de Chile, Casilla 487-3, Santiago, Chile

5 Instituto de Física, Pontificia Universidad Católica de Valparaíso, Casilla 4059, Valparaíso, Chile

Published online: 15 April 2026

filaments in gas discharges, smears in chemical reactions, optical patterns, oscillons in granular media, and isolated states in thermal convection, among others (see reviews [4–7, 15] and references therein).

The emergence of localized structures requires the coexistence of multiple states and a characteristic length scale that enables spatial confinement. The characteristic length is related to at least one equilibrium that has an inherent length, such as being a periodic solution (pattern) or having spatial oscillations in the connections between equilibria [4–7]. A representative model that incorporates these elements is the non-variational Swift–Hohenberg equation, widely used to describe the dynamics of systems close to Lifshitz points [16], where the emergence of spatial patterns and bistability converge. This equation has proven to be relevant in contexts as diverse as nonlinear optics [16, 17], chemical systems [17], elastic [18] and acoustic [19] media, and even in biological models [17]. A key aspect of this model is that the inclusion of non-variational terms can lead to a spontaneous breaking of spatial reflection symmetry. This symmetry breaking enables localized structures to undergo a transition from motionless to propagating states, where the initial condition selects the direction of motion. Such behavior has been both theoretically predicted and experimentally confirmed across several physical systems, including liquid crystals, chemical reactions, and various optical and mechanical settings [20–25]. On the other hand, macroscopic physical systems exhibit inherent fluctuations [26]. The presence of fluctuations generates random walks of the particle-like solutions.

Random motion has attracted the attention of the scientific community for centuries, with Brownian motion being the paradigmatic example [27, 28]. One of the main characteristics of this random walk is that the mean square displacement increases linearly with time. Movement of self-propelled objects, active matter, may exhibit non-Brownian random walks [28]. For example, bacteria such as Escherichia coli exhibit random movement, characterized by alternating straight-line forward motion with random turns, followed by further straight-line forward motion, continuously maintaining this alternating pattern [30, 31]. This dynamic is called *running and tumbling*. Indeed, Escherichia coli, whose non-Brownian motion alternates between ballistic and diffusive regimes [32]. Namely, its mean square displacement is characterized by an initially quadratic regime in time (ballistic) and subsequently replaced by a linear one (diffusive). These regimes represent two extremes in particle dynamics, characterized by predominantly constant or stochastic temporal rate. Kramers' theory explains how a particle or system crosses an energy barrier due to thermal noise. In the run-and-tumble framework, Kramers' theory describes the transition from the initial ballistic to the diffusive regime in the presence of noise and potential barriers, incorporating friction to explain how motion slows and becomes diffusive upon crossing these barriers.

Recent studies have analyzed the combined effect of parity symmetry breaking and multiplicative noise on the transition from a motionless to a traveling localized state. In this setting, the breaking of spatial reflection symmetry induces propagation in a preferred direction, while noise causes stochastic reversals in the direction of motion [29]. This interplay generates run-and-tumble dynamics, analogous to those observed in bacteria whose non-Brownian motion alternates between ballistic and diffusive regimes. A detailed study of the running and tumbling of particle-like solutions is necessary to understand their properties and the conditions required to observe them in different out-of-equilibrium physical systems.

This research aims to examine in detail the emergence of run-and-tumble dynamics in one-dimensional localized structures subject to random fluctuations. The analysis is performed using a stochastic, non-variational scalar model that exhibits localized structures that run and tumble. Noise is included in the parameter responsible for the transition between motionless and traveling states. Although the analyzed model lacks internal drivers or localized energy sources, the mechanism presented here—based on the interplay between nonlinearity, symmetry breaking, and a stochastic forcing—provides an effective description of behaviors typically associated with active systems driven internally. On long but finite time scales, the localized structures pre-sent three regimes: an initial diffusive regime, followed by a ballistic regime, and finally a diffusive one. Mean square displacement analyses reveal these regimes. To explain the run-and-tumble phenomenon, we derive a minimal model for the position and velocity of the localized structure. This reduced model accounts for the run-and-tumble dynamics of localized structures described by the scalar model. Note that this simple model allows for analytical analysis. The reduced model exhibits spontaneous parity-symmetry breaking and stochastic propagation reversals described by Kramers' law. Using this law, we estimate the mean first-passage time, consistent with simulations of the minimal model. Furthermore, we numerically solved the associated Fokker-Planck equation, recovering the key features of the emergent dynamics: the behaviors for finite long times, the noise-induced transition in the stationary velocity distribution, and a diffusion process at the particle position. Our results indicate that active behavior can arise generically in simple physical systems, without requiring specific active mechanisms, only symmetry breaking and noise.

The manuscript is organized as follows: In Section 2, we introduce the prototype model of localized structures; we show that this model exhibits running and tumbling of localized structures; and we further analyze the statistical properties of these phenomena. In Section 3, we propose a

minimal model for the particle-like solution by reducing it to the central manifold, using a Langevin-type equation. We also analyze the statistical properties of this model. From the Langevin-type equation, we derive and examine its associated Fokker-Planck equation. In the final Section, we present the conclusions and discuss future directions of this work.

2 Stochastic localized structure model

Localized structures require the simultaneous presence of multistability and a characteristic length [5]. These conditions arise naturally in the vicinity of a Lifshitz point [1], in which a spatial instability and the nascent of bistability occur simultaneously. A prototype model with a Lifshitz point that exhibits both localized and extended patterns is the Swift-Hohenberg equation [33]. This model is an isotropic, reflection-symmetric, and real-order-parameter nonlinear equation originally derived to describe pattern formation in Rayleigh-Benard convection [33]. A generalization includes an additional term that breaks the field-reflection symmetry, which is denominated as the non-variational Swift-Hohenberg equation [16, 17]. This generalization has been deduced in various field on nonlinear science, such as chemistry [17, 34], plant ecology [35], nonlinear elasticity [36], and nonlinear optics [16, 17]. Hence, the non-variational Swift-Hohenberg equation applies to a wide range of systems that undergo a spatial-symmetry-breaking instability, close to a second-order critical point marking the onset of a hysteresis loop.

Using scale separation techniques and normal form theory, close to a Lifshitz point, the dynamics of the system is described by [16, 17] (the non-variational Swift-Hohenberg equation)

$$\partial_t u = \eta + \mu u - u^3 - \nu\partial_x^2 u - \partial_x^4 u + 2bu\partial_x^2 u + \left[c + \sqrt{a}\xi(x,t)\right](\partial_x u)^2, \tag{1}$$

where $u = u(x,t)$ is an order parameter and denotes a scalar order field that can describe a variety of physical quantities, including amplitude enveloped of the light [16], chemical concentration[17], average molecular orientation [18], and radial displacement [19], surface radial displacement [36], among others. The parameter μ governs the bifurcation behavior of the system, whereas η modulates the extent of the bistable regime. The coefficient ν represents diffusion when negative and anti-diffusion when positive. Parameters b and c correspond to the contributions from nonlinear diffusion and advective transport, respectively. $\xi(x,t)$ is a Gaussian white noise with a mean value and a correlation function given by

$$\langle \xi(x,t)\rangle = 0, \tag{2}$$

$$\langle \xi(x,t)\xi(x',t')\rangle = \delta(t-t')\delta(x-x'), \tag{3}$$

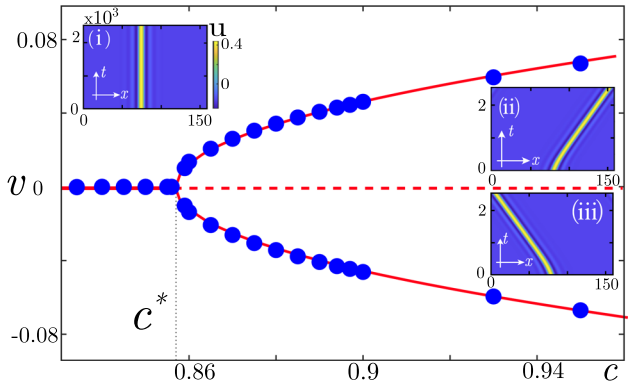

Fig. 1 Spontaneous symmetry breaking from motionless to traveling LSs exhibited by Eq. (1) as a function of nonvariational parameter c with $\eta = -0.02$, $\mu = -0.092$, $\nu = 1$, $b = -1.0$, $a = 0$, $\Delta x = 0.8$, and $\Delta t = 0.03$. The blue circles account for the numerical LS velocity, where the transition between motionless to traveling solutions occurs at $c^* = 0.855$. The corresponding left and right speed fittings (red hard curves) are given by $v_{R,L} = \pm v_0\sqrt{c^* - c}$ with $v_0 = 0.222$. The solid and dashed lines account for stable and unstable LS. The insets (i), (ii), and (iii) are the spatiotemporal evolution of the motionless, traveling towards the left and right flank LS, respectively

here the symbol $\langle\cdot\rangle$ represents the average over the noise realizations in both space and time. Consequently, the noise exhibits no temporal or spatial memory, and the parameter a is the noise level intensity. To numerically solve the stochastic partial differential Eq. (1) in a periodic domain with white noise, the space was discretized using central finite differences, applying periodicity as a boundary condition. The discretization transforms the partial equation into a system of ordinary differential equations; this system is integrated in time using a fourth-order Runge–Kutta scheme for the deterministic part, while the stochastic term is incorporated using the Euler–Maruyama method, generating independent Wiener increments with zero mean and variance Δt [37]. This scheme, based on the Itô interpretation, combines the accuracy of a fourth-order integrator with the simplicity of stochastic treatment. Finally, the simulations of model (1) were carried out using an observation timescale of the order 10^5 iterations, which allowed robust characterization of the noise-induced phenomena in the considered parameter region.

Figure 1 shows the bifurcation diagram of the localized structure speed v as a function of the non-variational parameter c without noise $a = 0$ of the model Eq. (1). Note that the speed of the localized structure v was calculated following the position of the maximum of the LS over time and determining its temporal variation. This diagram illustrates a transition from motionless to traveling localized states as the non-variational parameter c increases [25]. The insets (i), (ii), and (iii) show the spatiotemporal evolution of a stationary localized structure, which moves towards the right and left flanks when the parity-symmetry is broken, respec-

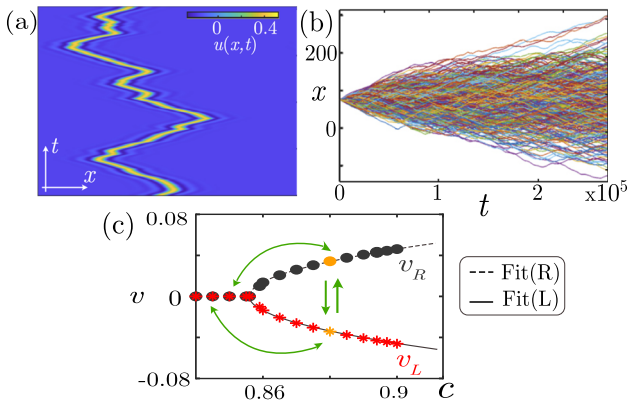

Fig. 2 Run-and-tumble behavior of LSs presented by numerical simulations of Eq. (1) for $\eta = -0.02$, $\mu = -0.092$, $\nu = 1$, $b = -1.0$, $c = 0.865$, $\Delta x = 0.8$, and $\Delta t = 0.03$. (a) Spatiotemporal evolution of a LS under the effect of Gaussian white noise fluctuations with a level intensity $a = 0.25$. (b) Temporal evolution of several LS realizations for the same initial condition. (c) Bifurcation diagram of the LS velocity as a function of non-variational parameter c. After the critical point c^*, black circles and red asterisks represent the right and left propagation velocities of a LS, respectively. Before the critical point, the circle and the asterisk collapse until the LS becomes motionless. The green arrows schematically show the noise-induced transitions between a static and an LS moving left or right, and vice versa

tively. By incorporating the influence of fluctuations on the nonlinear advection parameter c within regions exhibiting localized propagative structures, we numerically observe the emergence of running and tumbling behaviors in these localized structures. Figure 2(a) displays a representative example of the spatiotemporal dynamics associated with such stochastic localized structures. To analyze their statistical behavior, we consider a set of 600 realizations using an identical initial condition, as depicted in Fig. 2(b). Figure 2(c) presents the velocity of localized structures as a function of the nonvariational parameter c. The green arrows indicate noise-induced transitions between stationary states, localized structures moving either to the left or right, and reverse transitions between stationary states, localized structures moving either to the left or right, and reverse transitions.

2.1 Probability density function

In this section, we calculate the probability density function $P(x,t)$ and the mean square displacement In this section, we calculate the probability density function $P(x,t)$ and the mean square displacement $\mathrm{MSD}(t) = \langle (x(t) - x_0)^2 \rangle$ as a function of time t and x_0 denotes a reference position. Figure 3 summarizes the results for the evolution of the LS position obtained from ensembles of realizations corresponding to three different values of the parameter $c = \{0.850, 0.860, 0.865\}$. All numerical simulations for this study considered long but finite times. In this chart, the first, second, third, and fourth rows account for the three sets of realizations as a function of time, $P(x)$ denotes the time-marginalized probability density function (PDF) estimated by pooling all samples $x(t)$ over the entire time interval, the conditional probability density function $P(x,t|x_0,t_0)$ (CPDF), and the mean square displacement $\mathrm{MSD}(t)$ as a function of time, respectively. From the left and middle columns, we observe that the LS position presents a monomodal CPDF and an $\mathrm{MSD}(t)$ with two principal regimes: ballistic (t^2) and diffusive (t^1). The crossover time t_c—determined by the intersection of both regimes–delimits the timescale from which the noise interrupts the ballistic and gives way to a diffusion regime. From the right column, we can see that the LS position presents a bimodal CPDF and an $\mathrm{MSD}(t)$ with two principal regimes: superballistic $t^{2.9}$ and ballistic t^2. Hence, we conclude that the localized structures undergo a transition from a monomodal to a bimodal conditional probability density function. Note that this transition is observed at a finite final time $t_f = 3.5 \times 10^5$.

Figure 4(a) presents a more detailed analysis of the conditional probability density function for a finite final time $t = t_f$. The bifurcation diagram shows two distinct regimes depending on the parameters a and c. For $c < c^* = 0.855$, the distribution is monomodal (green stars), whereas for $c > c^*$, both monomodal (red squares) and bimodal (blue circles) distributions are observed. Figure 4(b) illustrates the evolution of the mean square displacement as a function of time, for $c = 0.865$ and four different values of noise intensity $a = \{10, 40, 160, 300\} \times 10^{-3}$. It is observed that for low values of a ($a < 0.04$) the system exhibits only ballistic regimes, while for higher values ($a > 0.04$), a diffusive behavior emerges at long timescales. On the other hand, the influence of the parameter c on the mean square displacement is further examined for a fixed noise intensity $a = 0.04$ and two representative values of $c = \{0.80, 0.865\}$, as shown in Fig. 4(c). It is observed that for $c < 0.87$, the probability density is monomodal. At the same time, for higher values it becomes bimodal, indicating a bifurcation related to the effective potential structure induced by the parameter c. This transition reflects a qualitative change in the stochastic trajectories of the system, where the probability is redistributed among multiple effective wells. Furthermore, when $c < c^*$, the mean square displacement exhibits a purely diffusive behavior on intermediate and long time scales, suggesting the absence of a preferred direction of motion and the predominance of noise-induced randomness. Conversely, for $c > c^*$, where the distribution becomes bimodal, the system may undergo partial confinement within multiple potential wells, resulting in an initial ballistic regime followed by slower diffusion.

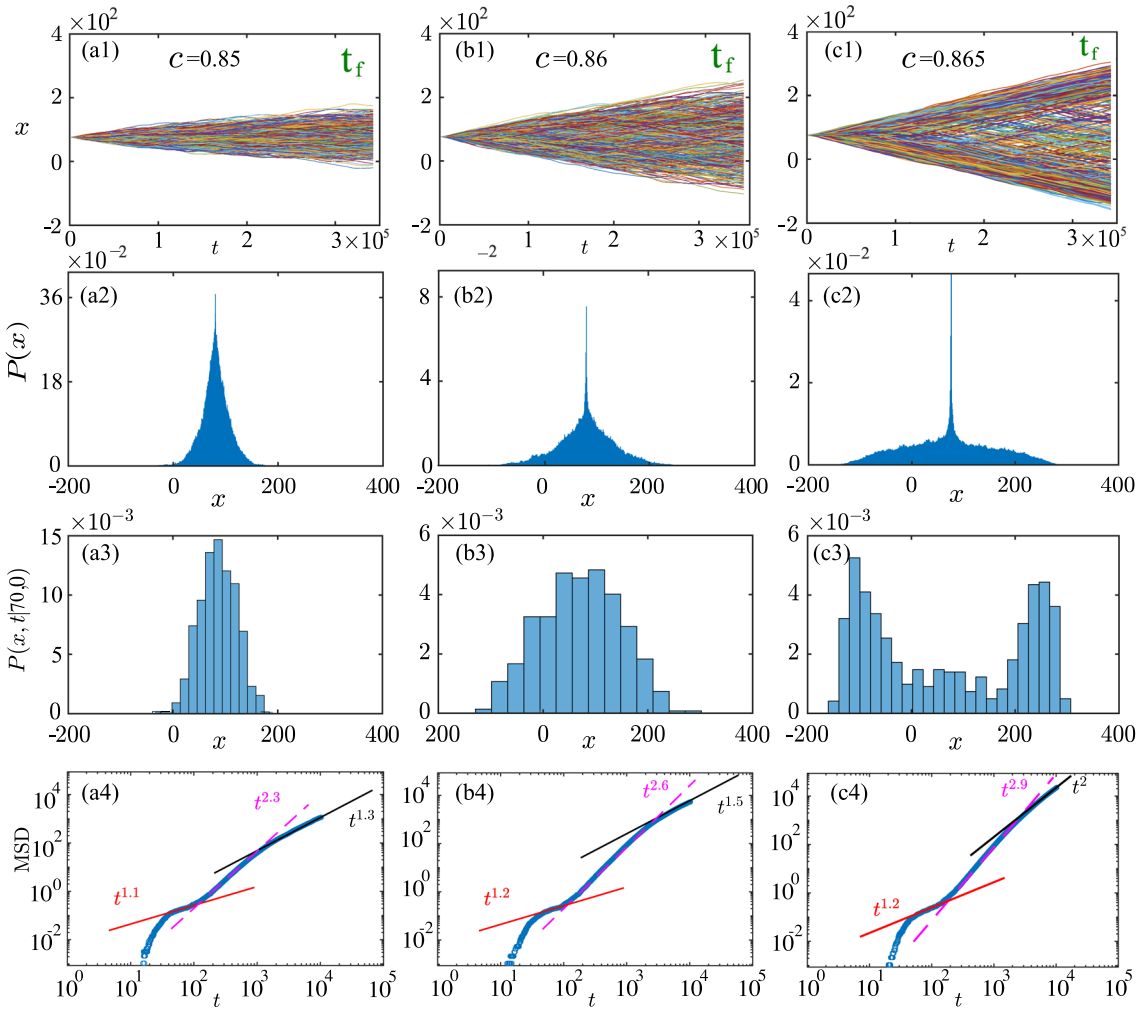

Fig. 3 Statistical analysis of localized structure dynamics using model (1) for three values of the parameter $c = \{0.850, 0.860, 0.865\}$, with fixed parameters: $a = 0.02$, $\eta = -0.02$, $\mu = -0.092$, $\nu = 1$, $b = -1.0$, $\Delta x = 0.8$, $\Delta t = 0.03$, and $t_f = 3.5 \times 10^5$. Columns (a)–(c) correspond to increasing values of parameter c: (a) $c = 0.850 < c^*$ (below bifurcation), (b) $c = 0.860 \approx c^*$, and (c) $c = 0.865 > c^*$ (above bifurcation). Each column includes four rows: (1) ensemble of the LS position realizations; (2) time-marginalized probability density function $P(x)$; (3) conditional probability density function at final time $P(x, t = t_f \mid 70, 0)$; and (4) mean square displacement as a function of time MSD(t)

2.2 MSD characterization

In this section, we characterize the time-marginalized probability density function $P(x)$ and the mean square displacement MSD(t) for each set of realizations corresponding to a noise level intensity a, where each set has 600 realizations (cf. Fig. 1). Figure 5(a) displays the set of realizations for three increasing values of noise intensity a, with the non-variational parameter fixed at $c = 0.865 > c^*$. For low noise levels, the system exhibits predominantly ballistic behavior, whereas for higher noise levels, the trajectories transition to a diffusive regime. The corresponding time-marginalized probability density function $P(x)$ is shown in Fig. 5(b). Note that the PDF also develops a different tail behavior as the parameter a increases. Figure 5(c) shows the MSD(t) for three different values of the parameter a, highlighting scaling exponents $\{\alpha, \beta, \gamma\}$. To characterize the different regimes, we can approximate the MSD by

$$\mathrm{MSD}(t) = \begin{cases} \sqrt{D}t^{\alpha}, & t \le t_1, \\ \sqrt{B}t^{\beta}, & t_1 \le t \le t_2, \\ \sqrt{F}t^{\gamma}, & t \ge t_2, \end{cases} \tag{4}$$

where t_1 and t_2 are the crossover times, and $t_2 = t_c$. The behavior of the exponents as a function of the noise level intensity a is displayed in Fig. 5(d). For noise levels below the critical threshold $a < a^* \approx 0.20$, all exponents converge toward a ballistic regime characterized by $\alpha \to 1.5$, $\beta \to 3$, and $\gamma \to 2$. Above the critical value, $a > a^*$, the exponents

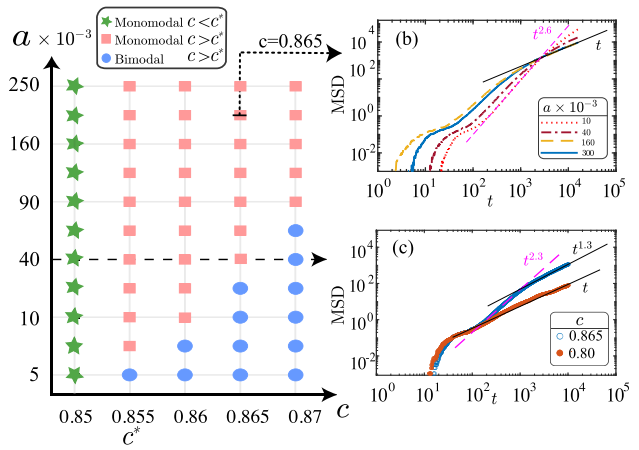

Fig. 4 Analysis of the condition probability density function $P(x, t = t_f|70, 0)$, obtained using the model (1) with the following parameter values $\eta = -0.02$, $\mu = -0.092$, $\nu = 1$, $b = -1.0$, $\Delta x = 0.8$, $\Delta t = 0.03$. Above the threshold $c > c^*$, red squares have a monomodal CPDF, while the blue circles represent a bimodal CPDF. (b) Time evolution of the mean square displacement for a fixed value of $c = 0.865 > c^*$ and three noise intensity values $a = \{0.2, 0.5, 1.0\}$. (c) Time evolution of the mean square displacement for a fixed value of $a = 0.04$ and two values of $c = 0.80$ (below the threshold) and $c = 0.865$ (above the threshold)

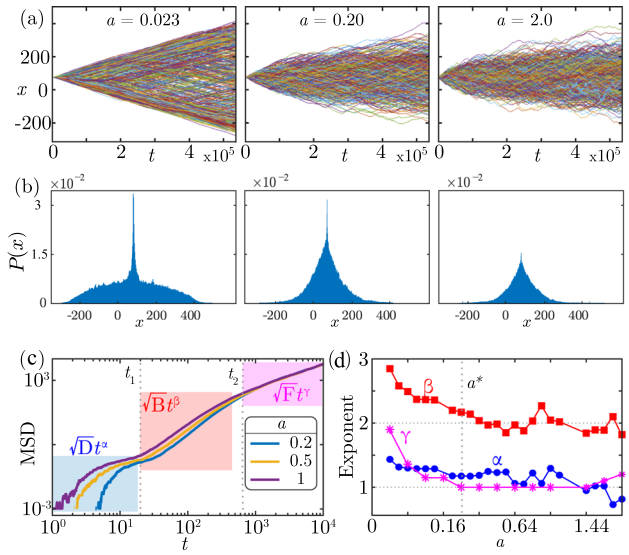

Fig. 5 Analysis of the $\{\alpha, \beta, \gamma\}$ MSD exponents as a function of the noise level intensity a, corresponding to the short-, intermediate-, and long-time regimes within the framework of model (1). The remaining parameters are fixed at $\eta = -0.02$, $\mu = -0.092$, $\nu = 1, b = -1.0, c = 0.865$, $\Delta x = 0.8$, $\Delta t = 0.03$, and $t_f = 10500$. (a) Sets of realizations and (b) time-marginalized probability density functions $P(x)$ for the position of the LS, corresponding to increasing noise intensity values $a = \{0.023, 0.2, 2.0\}$. (c) MSD as a function of time for three increasing values of intensity noise a with their respective regimes highlighted in the blue, red, and magenta squares. t_1 and t_2 are crossover times that account for the different regimes, respectively. (d) Exponents of the MSD $\{\alpha, \beta, \gamma\}$ as a function of noise intensity a. The vertical line denotes the threshold of exponents a^*

exhibit a transition: the exponent α remains slightly above 1, consistent with a Brownian process, while $\beta \to 2$ accounts for a ballistic regime and $\gamma \to 1$ a diffusive one.

In brief, the dynamics of the stochastic localized structure exhibit distinct propagation regimes, the nature of which depends on the noise level intensity. When this intensity exceeds a critical threshold $a > a_c$, the exponents reveal a transition from a ballistic behavior on intermediate time scales ($\beta \to 2$) to a diffusive regime on long times ($\gamma \to 1$). This scenario is consistent with that observed in active systems, such as bacteria that move along run-and-tumble trajectories [32].

3 Particle type description: minimal model

An effective description of the stochastic dynamics of LSs, i.e., the position and velocity, can be obtained following the perturbative approach used in Ref. [25], which considers the system near the transition from traveling to motionless LSs. In this framework, the bifurcation non-variational parameter is expanded as $c = c^* + \epsilon c_0$, with $\epsilon \ll 1$ small scaling parameter (cf. Fig. 1). Let us consider the ansatz

$$u(x,t) = u_{ls}\,(x - q(\epsilon t)) + \epsilon\, p(\epsilon^2 t) u_{as}\,(x - q(\epsilon t)) + w(x, q, p), \tag{5}$$

where $u_{ls}\,(x - q(\epsilon t)) \equiv |u_{ls}\rangle$ represents the symmetrical motionless localized structure at the critical point, and $u_{as}\,(x - q(\epsilon t)) \equiv |u_{as}\rangle$ accounts for the eigenfunction corresponding to the asymmetric critical mode of linearized operator associated to $u_{ls}(x)$. Namely, $u_{ls}(x)$ satisfies

$$0 = \eta + \mu u_{ls} - u_{ls}^3 - \nu \partial_x^2 u_{ls} - \partial_x^4 u_{ls} + 2b u_{ls} \partial_x^2 u_{ls} + c(\partial_x u_{ls})^2. \tag{6}$$

The $w(x, q, p) \equiv |w\rangle$ is a small nonlinear correction function that follows the scaling $w \ll \epsilon p \ll 1$. The variables $q(\epsilon t)$ and $p(\epsilon^2 t)$ account for the position of the LS and amplitude of the asymmetrical part. Note that the temporal scales of the position q and the amplitude p are different (cf. Ref. [25]). By replacing the above ansatz (5) in the corresponding model of Eq. (1), using Eq. (6), and linearizing in the perturbation w, we obtain the following expression after straightforward computations

$$\mathcal{L}|w\rangle = |B(q, p, \epsilon)\rangle, \tag{7}$$

where $\mathcal{L}$ is a linear operator given by

$$\mathcal{L} = (\ \mu - 3u_{ls}^2 - \nu\partial_x^2 - \partial_x^4 + 2b u_{ls}\partial_x^2) + 2c(\partial_x u_{ls})\partial_x \varphi + 2b(\partial_x^2 u_{ls}), \tag{8}$$

and $|B(q,\,p,\epsilon)\rangle$ represents the term arising from nonlinear interactions and perturbative contributions dependent on variables q, p, and the small parameter ϵ. Its explicit form is given by

$$\begin{aligned}|B\rangle = &-\epsilon\partial_z u_{ls}\dot{q} - \epsilon^2 p\partial_z u_{as}\dot{q} + \epsilon^3 u_{as}\dot{p}\\ &- [\mu\, u_{as} - 3u_{as}u_{ls}^2 - \nu\partial_z^2 u_{as} - \partial_z^4 u_{as} + 2bu_{ls}\partial_z u_{as}\\ &+\ 2a\xi\,\partial_z u_{as}\partial_z u_{ls} + 2b\partial_z^2 u_{ls}\,]\epsilon\; p - a\xi\,(\partial_z u_{as})^2\\ &- \left[2bu_{as}\partial_z^2 u_{ls} - 3u_{ls}u_{as}^2 + (c^* + a\xi)\,(\partial_z u_{as})^2\right]\epsilon^2 p^2\\ &+ \left[u_{as}^3 p^3 - 2pc_0\partial_z u_{as}\partial_z u_{ls}\right]\epsilon^3. \end{aligned} \tag{9}$$

Notice that the linear operator $\mathcal{L}$ has a kernel of dimension two that satiesfies $\mathcal{L}|\partial_z u_{ls}\rangle = 0$ and $\mathcal{L}^2|u_{as}\rangle = 0$ [25]. We have employed the standard notation $\dot{q} = \partial_t q$, $\dot{p} = \partial_t p$, and $z \equiv x - q(\epsilon t)$ that corresponds to the coordinate in the co-moving reference frame with speed $\epsilon\dot{q}$, and $c = c^* + \epsilon c_0$.

To solve the linear Eq. (7), the right-hand side of this equation must be in the image of the linear operator $\mathcal{L}$. To apply this condition, we use Fredholm's alternative or the solvability condition [3], which gives us a set of equations for the position $q(t)$ and critical mode $p(t)$. The solvability condition involves projecting Eq. (7) over the kernel of the adjoint operator $\mathcal{L}^\dagger$. Using the canonical inner product

$$\langle\langle f|g\rangle\rangle \equiv \int_{-\infty}^{\infty} f(x)g(x)dx, \tag{10}$$

and the solvability condition, this leads to the following equation for the particle type solution governing the slow dynamics (the minimal model)

$$\begin{aligned}\dot{p} &= \sigma\, p - p^3 + \sqrt{a_1}\eta(t),\\ \dot{q} &= -p + a_2\eta(t),\end{aligned} \tag{11}$$

where the bifurcation parameter is given by

$$\sigma \equiv 2\epsilon c_0 \frac{\langle\langle\psi_1 \mid \partial_x u_{as}\,\partial_x u_{ls}\rangle\rangle}{\langle\langle\psi_1 \mid u_{as}\rangle\rangle}, \tag{12}$$

and $\eta(t)$ is a Gaussian white noise with the following statistical properties

$$\langle\eta(t)\rangle = 0, \qquad \langle\eta(t)\eta(t')\rangle = \delta(t-t'). \tag{13}$$

The corresponding noise intensities are

$$\begin{aligned}a_1 &= \frac{a^2}{\epsilon^4\langle\langle\psi_1 \mid u_{as}\rangle\rangle^2},\\ a_2 &= -\frac{a}{\epsilon\langle\langle\psi_0 \mid \partial_x u_{ls}\rangle\rangle}\frac{\langle\langle\psi_0\psi_1 \mid (\partial_x u_{ls})^4\rangle\rangle}{\langle\langle\psi_1^2 \mid (\partial_x u_{ls})^4\rangle\rangle},\end{aligned} \tag{14}$$

where ψ_0 and ψ_1 are the adjoint eigenfunctions associated with the translational and asymmetric modes, respectively. That is, $\mathcal{L}^\dagger\langle\psi_0| = 0$ and $\mathcal{L}^\dagger\langle\psi_1| = 0$. Note that $\{\langle\psi_0|, \langle\psi_1|, |u_{as}\rangle\}$ are determined numerically [25]. Observed that these equations are obtained at the same order in ϵ.

Hence, the dynamics of LSs are governed by a Langevin equation for the velocity p, subject to a symmetric bistable potential $U(p) = -\sigma\, p^2/2 + p^4/4$, which exhibits minima at $\pm\sqrt{\sigma}$. Importantly, the position and velocity of the LS are connected through a stochastic differential equation; however,their relationship cannot be reduced to a simple kinematic definition, in contrast to the Langevin classical description. The reduced dynamical model Eq. (11), starting from the resting configuration $p(0) = 0$, initially describes how the LS acquires a velocity toward one of the flanks (corresponding to a minimum of the potential) and begins to fluctuate around that velocity [$t \le t_2$ in Fig. 5(c)]. Subsequently, for times comparable to the mean first passage time, the LS may stop and reverse its propagation direction [$t \ge t_2$ in Fig. 5(c)] and again perform this dynamic cycle (run-and-tumble), as illustrated in Fig. 2(a). From this model and the noise-induced transition phenomenon [38], one expects that trajectories present a running and tumbling behavior.

Figure 6 shows the numerical results of a study on the reduced Eq. (11), equivalent to the analysis carried out for the spatiotemporal model Eq. (1), and illustrates the time evolution of the LS position based on ensembles of 600 realizations. All simulations of this model were carried out using the Euler-Maruyama me-thod. For two values of the noise parameter, $a_1 = \{0.0015,\ 0.003\}$, panels (a1)-(b4) display, respectively: the LS trajectories over time, the time-averaged probability density $\langle P(x)\rangle$, the conditional probability density function $P(x, t \mid x_i = 70, t_0 = 0)$, and the mean square displacement MSD(t). The left and right columns correspond to the dynamics of the LS below and above the threshold $a_1 = a_1^* = 0.002$. In the left column, the LS exhibits a bimodal CPDF and an MSD(t) characterized by two regimes: superballistic ($t^{2.6}$) and ballistic (t^2). In contrast, the right column shows a monomodal CPDF and an MSD(t) with ballistic (t^2) and diffusive (t^1) behavior. Finally, Fig. 6(b4) shows a vertical dashed line indicating the numerical crossover time between the ballistic and diffusive regimes, $\tau_{kn} \sim 10^2$, which depends on the noise level intensity a_1. From the reduced Eq. (11), we estimate this crossover time analytically using Kramers' theory in the high-friction limit. The mean first passage time is given by $\tau_k = 2\pi\gamma/\left(\sqrt{U''(p_a)\,|U''(p_b)|}\right)e^{\Delta U/D}$, where D is the noise intensity, $\Delta U = U(p_b) - U(p_a)$ is the potential barrier height, and p_a, p_b are the minimum of the potential U and transition points, respectively [39]. This expression provides the characteristic time required for a particle to escape

from a metastable minimum under the condition $\Delta U \gg D$. Applying Kramers theory to our case (11), we obtain the following expression

$$\tau_k = \frac{\sqrt{2}\pi}{\sigma} \exp\left[\frac{\sigma^2}{4a_1}\right], \tag{15}$$

which is in agreement with the numerical results of crossover time $\tau_k \sim \tau_{kn}$. The overall scenario is summarized in the bifurcation diagram shown in Fig. 6(c) for finite long times. For $\sigma < 0$, the system exhibits monomodal probability densities with Brownian-like dynamics (green stars), whereas for $\sigma > 0$, both bimodal (blue circles) and monomodal (red squares) densities are found. In this latter regime, the solutions undergo a noise-induced transition from a bimodal density with ballistic exponents to a monomodal one with diffusive exponents at finite long times.

These observations indicate that the localized structures undergo a transition from a monomodal to a bimodal conditional probability density function for a finite final time $t = t_f$, consistent with the behavior exhibited by the spatiotemporal model Eq. (1). Consequently, the reduced model Eq. (11) proves effective in capturing the main dynamical features of the localized structures governed by the stochastic non-variational Swift–Hohenberg equation (1).

3.1 Fokker planck approach

In addition to the numerical simulations of the reduced Langevin-like Eq. (11), we consider the associated Fokker-Planck equation to study the time evolution of the conditional probability density function $P(q, p, t|q_0, p_0, t_0)$, where $\{q, p\}$ and $\{q_0, p_0\}$ denote the position and velocity in the time t and t_0, respectively. The corresponding Fokker—Planck equation is given by [26]

$$\frac{\partial P}{\partial t} = -\frac{\partial}{\partial p}\left[(\sigma p - p^3)\, P\right] + p\,\frac{\partial P}{\partial q} + \frac{a_1}{2}\frac{\partial^2 P}{\partial p^2} + \sqrt{a_1}a_2\frac{\partial^2 P}{\partial q\,\partial p} + \frac{a_2^2}{2}\frac{\partial^2 P}{\partial q^2}. \tag{16}$$

This equation accounts for the conditional probability density function given by an initial distribution condition $f(q_0, p_0) = P(q_0, p_0, t_0|q_0, p_0, t_0)$. Note that when $t \to \infty$, the joint probability density function converges to the stationary probability. The Fokker-Planck Eq. 16 is numerically studied using the finite symmetrical differences code to conserve the total probability with the Runge-Kutta order-4 algorithm and using periodic boundary conditions.

Figure 7 shows a time series of a colormap of the joint probability density function obtained from numerical solution of Eq. (16) for $\sigma = 0.35$. Panel (a) corresponds to the initial condition, where the joint probability density functions are given by a narrow Gaussian localized in both q and p. As time evolves, the joint probability density function

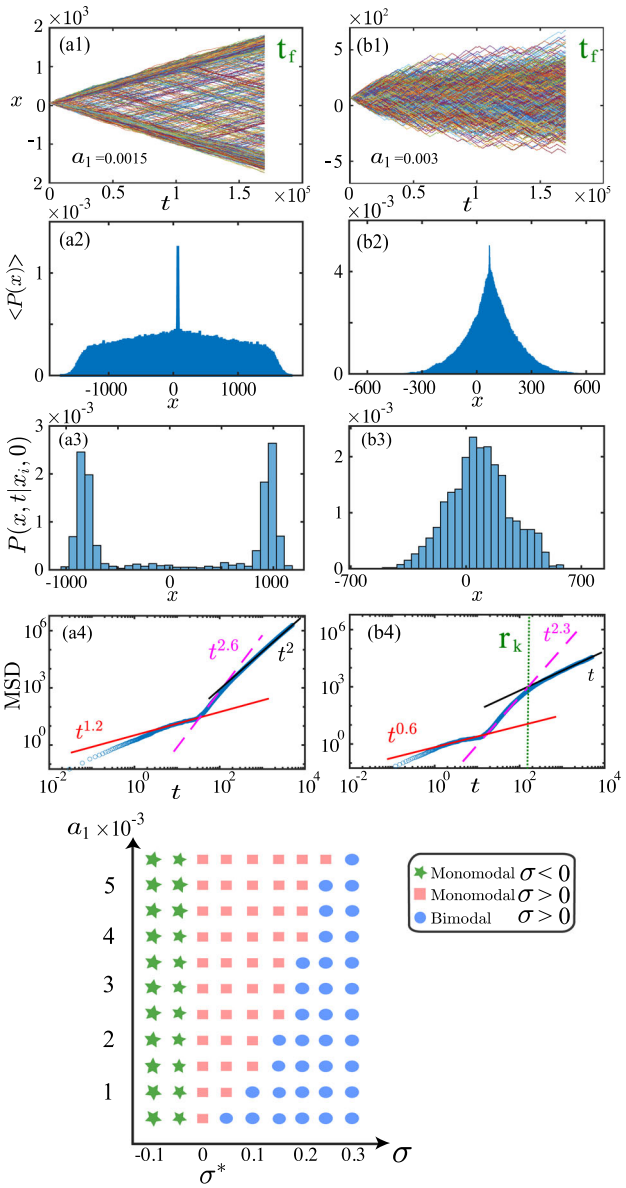

Fig. 6 Statistical characterization of the ensemble of localized structure positions obtained from the minimal model (11) for the particle type solution with fixed parameters $a_2 = 1.3$ and $\Delta t = 0.03$. For two values of the noise level intensity $a_1 = \{0.0015, 0.003\}$ and with $\sigma = 0.15$, columns (a)–(b) correspond to increasing values of parameter a_1: (a) $a_1 = 0.0015 < a_1^*$ (below bifurcation) and (b) $a_1 = 0.003 > a_1^*$ (above bifurcation). Each column includes four rows: (1) ensemble of the LS position realizations; (2) time-marginalized probability density function $P(x)$; (3) CPDF at final time $P(x, t = t_f \mid x_i, 0)$; and (4) mean square displacement as a function of time MSD(t). (c) The bifurcation diagram illustrates the dependence of the noise level intensity a_1 on the control parameter σ. Below the threshold $\sigma < 0$, green stars represent a monomodal CPDF. Above the threshold $\sigma > 0$, red squares have a monomodal CPDF, while the blue circles represent a bimodal CPDF

spreads. Panels (b) and (c) show the intermediate ballistic regime, where $P(q, p, t|0, 0, 0)$ exhibits clear bistability in both variables, with two dominant peaks emerging along both q and p axes. These results are consistent with the numerical simulations of the non-variational Swift–Hohenberg Eq. (1) and its reduced model (11) for long but finite times (see the region of blue circles in Figs. (4) and (6), respectively). At longer times, as shown in panel (d), the system reaches a stationary regime due to the boundary conditions, characterized by a stationary distribution that approximately factorizes as $P_s(q, p) \approx P_s(q)\, P_s(p)$. The marginal density $P_s(p)$ reflects the bistable character of the system, with two peaks located near the minima of the effective potential $U(p)$, consistent with the double-well structure for $\sigma > 0$. On the other hand, the marginal distribution $P_s(q)$ becomes uniform, indicating that the position of the LS undergoes long-time diffusion (see the region of square red in Figs. (4) and (6)). It is important to note that once the stationary distribution is reached, the stochastic transition from biomodal to monomodal behavior observed in the position x is no longer present. The noise-induced transition is instead captured in the stationary probability density associated with the velocity variable p.

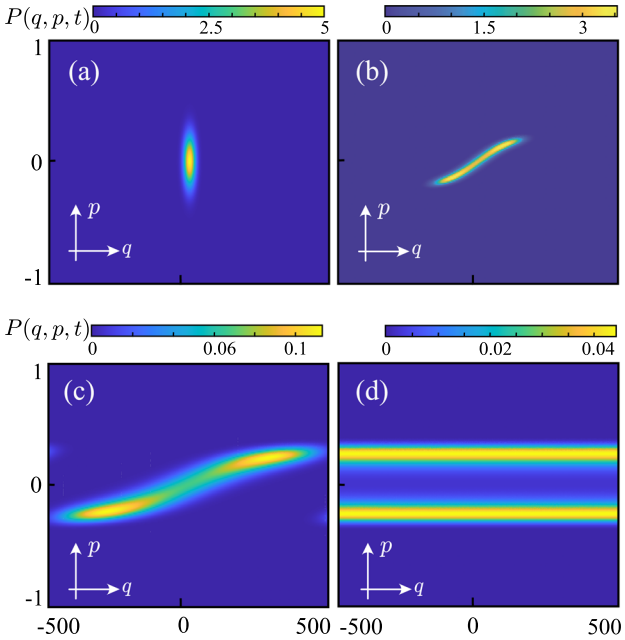

Fig. 7 Time evolution of the conditional probability density function $P(q, p, t)$ obtained from the numerical integration of the Fokker—Planck equation (16) with parameters $\sigma = 0.35$, $a_1 = 0.05$, $a_2 = 1.1$, time step $\Delta t = 0.01$, and spatial discretization $\Delta q = \Delta p = 1.0$. (a) Initial condition: narrow Gaussian localized in both q and p. (b) Short-time evolution showing spreading of the distribution. (c) Intermediate ballistic regimen where bimodality emerges in the velocity marginal $P(p, t)$. (d) Stationary regime that account for a diffusive dynamics: the marginal density $P_s(p)$ becomes bimodal, reflecting the double-well structure of the effective potential, while $P_s(q)$ approaches a uniform distribution, consistent with long-time diffusion in position

4 Conclusions and perspectives

This work demonstrates that LSs can develop run-and-tumble dynamics without requiring living components or internal propulsion mechanisms. This type of dynamics arises naturally when three fundamental ingredients combine: nonlinearity, parity-breaking symmetry, and noise. Through statistical analysis of mean square displacement for long but finite times, we observe a sequence of dynamical regimes: initial diffusion, intermediate ballistic, and long-time diffusion. These regimes are characterized by monomodal and bimodal probability density functions for the LS position. To understand the origin of these dynamics, we derive an effective minimal model, Langevin approach, that describes the evolution of the LS's position and velocity as a particle in a velocity-symmetric bistable potential landscape perturbed by noise. This reduced model follows a double-well Langevin-type equation in which the velocity can reverse upon overcoming energy barriers. The transition between left- and right-moving states follows Kramers' law. This prediction quantitatively agrees with direct simulations of both the reduced model and the original system. Furthermore, by solving the Fokker-Planck equation associated with the reduced model, we thoroughly verify the dynamic behavior. The bimodal shape of the velocity stationary distribution confirms the existence of metastable states of persistent motion, and the transition between diffusive and ballistic regimes is faithfully reproduced in this theoretical framework.

Our results show that active particle-like behavior is not exclusive to complex living systems. This work proposes a general and robust mechanism for generating run-and-tumble dynamics in non-equilibrium systems, opening new avenues for controlling and understanding structural transport in optical, chemical, and active-matter media. In particular, in delayed optical cavity solitons, the transition from motionless to traveling solitons has been theoretically predicted [40], which may be relevant for optical memory applications [41]; the inclusion of fluctuations inherent in these optical systems may be responsible for the run-tumble dynamics of cavity solitons. Likewise, thermal effects in semiconductor microcavities can induce transitions from motionless to traveling localized states in one- and two-dimensional optical configurations [42–44]. Experimentally, a transition from motionless to traveling solutions has been observed; self-organized, solitary current filaments have been observed in a planar DC gas discharge system with a high ohmic resistance barrier (see Review [6] and references therein). Due to noise, the current filaments exhibit complex, random trajectories; more careful studies are required to determine the nature of the dynamics observed in these systems.

In extended systems, a fundamental question remains: how to determine the transition times between noise-induced equilibrium states (Kramer's law for extended states). In our work, because the dynamics of particle-like solutions are projected onto the central position-velocity manifold (minimal model), the field is described by ordinary differential equations, and the noise-induced transition has analytical expressions. This reduction is fundamental to conducting this analysis. Our results may provide new insights into the theory of noise-induced transitions in stochastic fields.

Author Contributions M.G.C. Conceptualization, Supervision; F.R.H. Writing – Original Draft, Software, Visualization; K.A.B. Simulation Development, Visualization; R.G.R. Supervision and Analysis; All Authors Reviewed and Edited the Manuscript.

Funding F.R.H. acknowledges support from the Dirección general de investigación e innovación de la Universidad de Tarapacá, Arica, Chile, under the Proyecto UTA Mayor N° 4741-25 and FONDECYT project N°1252227. K.A.-B. acknowledges INCIBE/URJC Agreement M3386/ 2024/ 0031/001 within the framework of the Recovery, Transformation and Resilience Plan funds of the European Union (Next Generation EU). M.G.C. acknowledges the financial support of ANID-Millennium Science Initiative Program-ICN17_012 (MIRO). R.G.R. thanks to FONDECYT N°1252227.

Data Availability Data will be made available on request

Declarations

Conflicts of Interest The authors declare that they have no conflict of interest.

References

1. Cross, M.C., Hohenberg, P.C.: Pattern formation outside of equilibrium. Rev. Mod. Phys. **65**, 851 (1993)
2. Coullet, P.: Localized patterns and fronts in nonequilibrium systems. Int. J. of Bifurcation Chaos **12**, 2445 (2002)
3. Pismen, L.M.: Patterns and Interface in Dissipative Dynamics. Springer, Berlin (2006)
4. Dissipative Solitons: From Optics to Biology and Medicine, Lecture Notes in Physics, Vol. 751, edited by N. Akhmediev and A. Ankiewicz (Springer, Heidelberg, 2008)
5. Localized States in Physics: Solitons and Patterns, edited by O. Descalzi, M. Clerc, S. Residori, and G. Assanto (Springer, New York, 2010)
6. Purwins, H.G., Bödeker, H.U., Amiranashvili, S.: Dissipative solitons. Adv. Phys. **59**, 485 (2010)
7. Knobloch, E.: Spatial localization in dissipative systems. Annu. Rev. Condens. Matter Phys. **6**, 325 (2015)
8. Marchetti, M.C., Joanny, J.F., Ramaswamy, S., Liverpool, T.B., Prost, J., Rao, M., Simha, R.A.: Hydrodynamics of soft active matter. Rev. Mod. Phys. **85**, 1143 (2013)
9. J. Scott Russell, Report on Waves, Report of the 14th meeting of the British Association for the Advancement of Science, Plates XLVII-LVII (York, 1844), pp. 311-390
10. Newell, A.C.: Solitons in Mathematics and Physics. Society for Industrial and Applied Mathematics, Philadelphia (1985)
11. Remoissenet, M.: Waves Called Solitons: Concepts and Experiments. Springer Science & Business Media, Heidelberg (2013)
12. Rajaraman, R.: Solitons and instantons, An introduction to solitons and instantons in quantum field theory. Elsevier, North-Holland, Amsterdam (1982)
13. Taylor, J.R.: Optical solitons: theory and experiment. Cambridge University Press, Cambridge (1992)
14. Nicolis, G., Prigogine, I.: Self-Organization in Non-Equilibrium Systems: From Dissipative Structures to Order through Fluctuations. J. Wiley and Sons, New York (1977)
15. P. Umbanhowar, F. Melo, and H. Swinney, Localized excitations in a vertically vibrated granular layer, Nature **382** (1996)
16. Clerc, M.G., Residori, S., Petrossian, A.: Bouncing localized structures in a Liquid-Crystal-Light-Valve experiment. Phys. Rev. E **71**, 015205(R) (2005)
17. Kozyreff, G., Tlidi, M.: Nonvariational real Swift-Hohenberg equation for biological, chemical, and optical systems. Chaos **17**, 037103 (2007)
18. Stoop, N., Lagrange, R., Terwagne, D., Reis, P.M., Dunkel, J.: Curvature-induced symmetry breaking determines elastic surface patterns. Nat. Mater. **14**, 337 (2015)
19. Perez-Arjona, L., Sanchez-Morcillo, V.J., de Valcarcel, G.J.: Ultrasonic cavity solitons. Europhys. Lett. **82**, 10002 (2008)
20. Coullet, P., Lega, J., Houchmandzadeh, B., Lajzerowicz, J.: Breaking chirality in nonequilibrium systems. Phys. Rev. Lett. **65**, 1352 (1990)
21. J. M. Gilli, M. Morabito, and T. Frisch, Ising-Bloch transition in a nematic liquid crystal. J. Phys, II (France) **4**, 319 (1994)
22. Haim, D., Li, G., Ouyang, Q., McCormick, W.D., Swinney, H.L., Hagberg, A., Meron, E.: Breathing spots in a reaction-diffusion system. Phys. Rev. Lett. **77**, 190 (1996)
23. Michaelis, D., Peschel, U., Lederer, F., Skryabin, D.V., Firth, W.J.: Universal criterion and amplitude equation for a nonequilibrium Ising-Bloch transition. Phys. Rev. E **63**, 066602 (2001)
24. Clerc, M.G., Coulibaly, S., Laroze, D.: Non-variational Ising-Bloch transition in parametrically driven systems. Int. J. Bifurcation Chaos Appl. Sci. Eng. **19**, 2717 (2009)
25. Alvarez-Socorro, A.J., Clerc, M.G., Tlidi, M.: Spontaneous motion of localized structures induced by parity symmetry breaking transition. Chaos **28**, 053119 (2018)
26. Gardiner, C.: Stochastic Methods: A Handbook for the Natural and Social Sciences. Springer-Verlag, Berlin Heidelberg (2009)
27. Mörters, P., Peres, Y.: Brownian motion. Cambridge University Press, Cambridge (2010)
28. Berg, H.C.: Random walks in biology. Princeton University Press, Princeton, New Jersey (1983)
29. Humire, F.R., Alfaro-Bittner, K., Clerc, M.G., Rojas, R.G.: Running and Tumbling Localized Structures: A Non-Brownian Motion. Phys. Rev. Lett. **133**, 207202 (2024)
30. DiLuzio, W.R., Turner, L., Mayer, M., Garstecki, P., Weibel, D.B., Berg, H.C., Whitesides, G.M.: Escherichia coli swim on the right-hand side. Nature **435**, 1271 (2005)
31. Jaan, M., Driessen, R., Galajda, P., Keymer, J.E.: and Cees Dekker, Bacterial growth and motility in sub-micron constrictions. Proc. Natl. Acad. Sci. **106**, 14861 (2009)
32. Xiao-Lun, W., Libchaber, A.: Particle diffusion in a quasi-two-dimensional bacterial bath. Phys. Rev. Lett. **84**, 3017 (2000)
33. Swift, J., Hohenberg, P.C.: Effects of additive noise at the onset of Rayleigh-Bénard convection Phys. Rev. A **15**, 319 (1977)
34. M'F. Hilali, G. Dewel, and P. Borckmans, Subharmonic and strong resonances through coupling with a zero mode Phys. Lett. A 217, 263 (1996)
35. Lefever, R., Barbier, N., Couteron, P., Lejeune, O.: Deeply gapped vegetation patterns: On crown/root allometry, criticality and desertification. J. Theor. Biol. **261**, 194 (2009)
36. Stoop, N., Lagrange, R., Terwagne, D., Reis, P.M., Dunkel, J.: Curvature-induced symmetry breaking determines elastic surface patterns. Nat. Mater. **14**, 337 (2015)

37. Kloeden, P.E., Platen, E.: Numerical Solution of Stochastic Differential Equations. Springer, Berlin (1992)
38. Transitions, N.-I.: Theory and Applications in Physics, Chemistry, and Biology, Werner Horsthemke and René Lefever. Springer, Berlin, Heidelberg (1984)
39. Hänggi, P., Talkner, P., Borkovec, M.: Reaction-rate theory: fifty years after Kramers. Rev. Mod. Phys. **62**, 251 (1990)
40. Tlidi, M., Vladimirov, A.G., Pieroux, D., Turaev, D.: Spontaneous motion of cavity solitons induced by a delayed feedback. Phys. Rev. Lett. **103**, 103904 (2009)
41. Barland, S., Tredicce, J.R., Brambilla, M., Lugiato, L.A., Balle, S., Giudici, M., Maggipinto, T., Spinelli, L., Tissoni, G., Knödl, T., Miller, M., Jäger, R.: Cavity solitons as pixels in semiconductor microcavities. Nature **419**, 699 (2002)
42. Spinelli, L., Tissoni, G., Lugiato, L.A., Brambilla, M.: Thermal effects and transverse structures in semiconductor microcavities with population inversion. Phys. Rev. A **66**, 023817 (2002)
43. Scroggie, A.J., McSloy, J.M., Firth, W.J.: Self-propelled cavity solitons in semiconductor microcavities. Phys. Rev. E **66**, 036607 (2002)
44. Kheradmand, R., Lugiato, L.A., Tissoni, G., Brambilla, M., Tajalli, H.: Rotating and Fugitive Cavity Solitons in semiconductor microresonators. Opt. Express **11**, 3612 (2003)